RSC Advances

PAPER

View Article Online
View Journal | View Issue

Cite this: *RSC Adv.*, 2025, **15**, 48978

Integrating network pharmacology, molecular docking and experimental validation to explore therapeutic targets for alleviating allergic rhinitis with anxiety and depressive behaviors

Yiyi Lin,†[a] Shihan Liu,†[a] Zhiquan Zhu,†[c] Jinxiong Yang,[a] Pan Huang,[c] Yuyang Liu*[b] and Wenlong Luo *[a]

Received 26th November 2025
Accepted 2nd December 2025

DOI: 10.1039/d5ra09128d

rsc.li/rsc-advances

Allergic rhinitis (AR) represents an inflammatory disorder affecting the nasal mucosa, triggered by exposure to allergens. This pathological process is often followed by olfactory hypofunction and depression. The therapeutic application of Traditional Chinese Medicine (TCM) is gaining increasing recognition, particularly in the context of treating AR. Although Xiaochaihu Decoction (XCHD) is recognized as a classic formula within the Treatise on Febrile Diseases and exhibits antidepressant properties, its specific function in AR has yet to be elucidated. *In vivo*, animal experiments confirmed that XCHD ameliorated neuroinflammation in the olfactory bulb based on restoration of the nasal mucosal barrier. Behavioral experiments further verified that XCHD alleviated depression behavior and olfactory impairment in mice. Combined with the molecular docking results and component target screening, the experimental results indicate that XCHD is critical in treating AR and is expected to be a candidate for treating impaired olfactory function and depression.

1 Introduction

As a chronic upper respiratory tract disorder, AR manifests through nasal symptoms including pruritus, paroxysmal sneezing, congestion, and hypersecretion, affecting about 10–40% of the global population.[1,2] The recurrent nasal symptoms of AR not only predispose patients to complications like asthma, but are also frequently accompanied by olfactory dysfunction (OD).[3,4] AR severely affects patients' daily lives and work performance, placing a considerable economic burden on both individuals and society.[5] Therefore, better therapeutic management strategies for AR are urgently needed.

Epidemiological data suggests that OD may occur in 10–88% of AR patients.[6] Moreover, OD promotes the progression of AR. Olfactory dysfunction is not only a loss of sensory function but is also related to the patient's emotional state and social interactions.[7] Thus, a diminished or lost sense of olfactory sensation reduces quality of life and may lead to depression. Epidemiological evidence confirms AR's strong linkage with mental health comorbidities, specifically anxiety and depressive states.[8,9] One cross-sectional study demonstrated the extent of this association: anxiety affected 45.9% of individuals with AR, while depression affected 35.7%. In comparison, the control group showed considerably lower prevalence rates of 10.4% for anxiety and 16.6% for depression.[10]

Recent research indicates that traditional Chinese medicine (TCM) could offer therapeutic benefits for AR. XCHD a classic formula documented in the TCM treatise Shang Han Lun, is commonly used for its therapeutic effects against inflammation, fever, and pain.[11–13] As research into the integration of Chinese and Western medicine advances, significant interest has focused on the pharmacological mechanisms of XCHD and its potential therapeutic applications for mood disorders like anxiety and depression. Evidence suggests that XCHD can mitigate signs of depression in rats experiencing chronic unpredictable stress. Several mechanisms may contribute to this benefit, including hypothalamic–pituitary–adrenal axis regulation, enhanced hippocampal neurotrophic factor synthesis, and monoaminergic neurotransmitter homeostasis.[14,15] Meanwhile, the clinical study found that XCHD combined with conventional antidepressants could alleviate the symptoms of depression in patients.

Although XCHD possesses recognized bioactivities including oxidative stress inhibition and anxiety suppression, critical

[a]*Department of Otorhinolaryngology, The Second Affiliated Hospital of Chongqing Medical University, Chongqing, China. E-mail: 300654@hospital.cqmu.edu.cn; Tel: +86 62887808*

[b]*Affiliation Department of Pathology, The Second Affiliated Hospital of Zunyi Medical University, Zunyi City, Guizhou Province, China. E-mail: 441085695@qq.com; Tel: +86 27596224*

[c]*State Key Laboratory of Trauma, Burn and Combined Injury, Department of Orthopedics/Sports Medicine Center, First Affiliated Hospital of Army Medical University, Chongqing, 400038, China*

† Co-first Author.

evaluation of its anti-allergic rhinitis mechanisms remains pending. Network pharmacology can predict and analyze the pharmacological mechanisms of drugs. At the same time, molecular docking serves to further validate drug function and mechanism by elucidating the binding modes and quantifying the binding free energies of drug molecules with their protein targets.[16] Integrating these approaches enables the identification of XCHD's biological targets in treating AR and its associated signaling pathways.

This research evaluates XCHD's therapeutic effects on AR, with a specific emphasis on alleviating AR-induced anxiety and depressive-like behaviors. Integrating network pharmacology predictions with structure-based docking simulations and murine assays, we identified the pharmacological effects of XCHD and the key molecular pathways that exert the effects. Specifically, we hypothesized that XCHD exerts a crucial role in AR-induced olfactory dysfunction and depressive-like behaviors through the PI3K-Akt pathway. Therefore, this research offers encouraging pharmacological and psychological approaches for allergic rhinitis patients, presenting additional options for AR treatment (Scheme 1).

2 Methods and materials

2.1 Animal models

Seven-week-old male C57BL/6J mice were acclimatized in an animal facility for 1 week. During the 14-day sensitization phase (days 1–14), mice assigned to the AR group received intraperitoneal injections of 200 μL saline containing 40 μg OVA and 2 mg aluminum hydroxide every other day. The control group received isovolumetric sterile saline (0.9% NaCl) injections under identical administration protocols. Daily nasal administration of 20 μL of 5% OVA dissolved in saline was performed per nostril in AR group mice throughout the excitation phase, beginning on day 15. The control group was given equal saline in the same manner. The Animal Ethics Committee of Chongqing Medical University reviewed and approved the animal experiment protocol (IACUC-SAHCQMU-2023-0069).

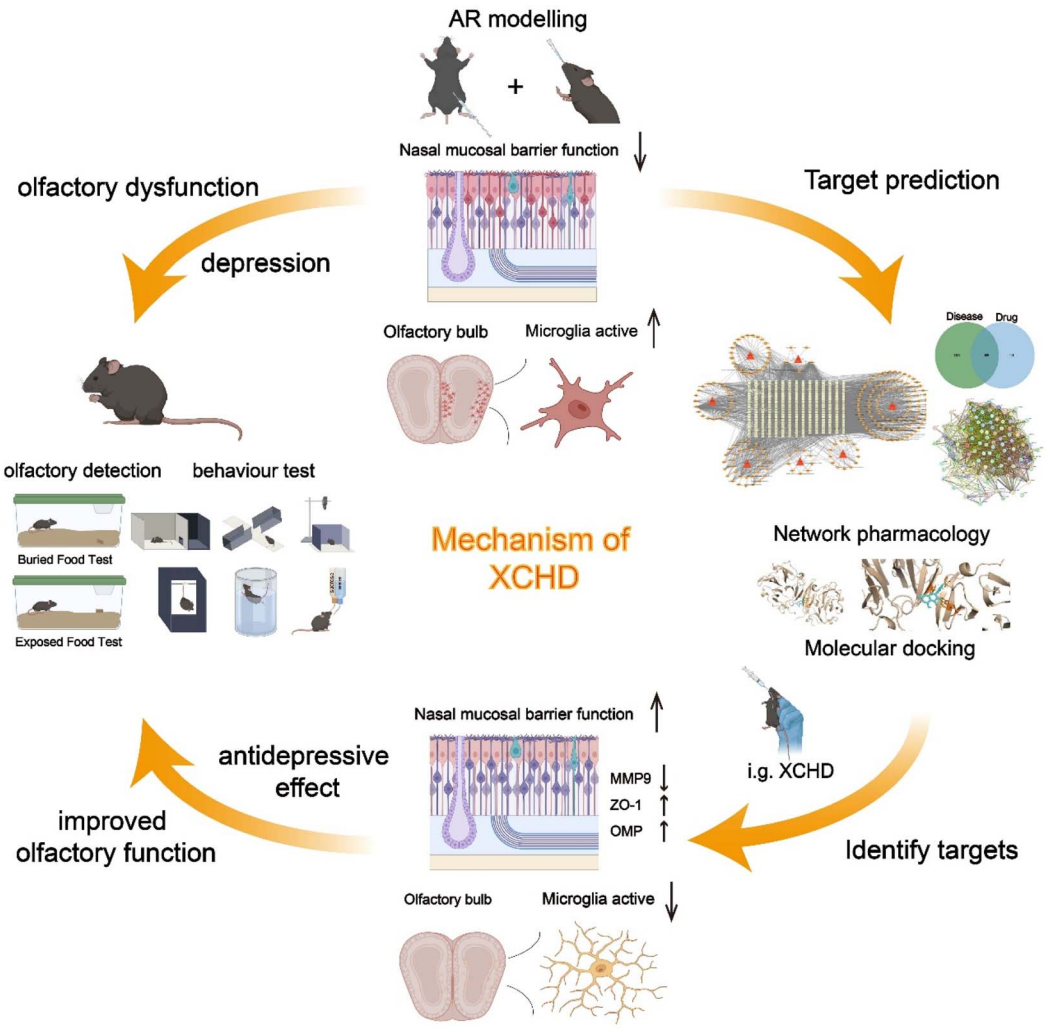

Scheme 1 Experimental procedure flowchart. Histological and behavioral experiments validate that XCHD restores the nasal mucosal barrier by modulating potential therapeutic targets for AR, thereby reducing inflammation levels in the nasal cavity and olfactory bulb. This mechanism alleviates olfactory dysfunction and emotional disturbances in AR mice.

After model establishment, mice were randomly assigned to groups. AR mice received XCHD treatment, while the PI3Ki group mice were administered LY294002 (MedChemExpress) *via* intraperitoneal injection at 10 mg per kg per day.

To determine whether the AR modeling was successful, after the last nasal administration, observers recorded the mice's nasal symptoms, including the number of times the mice scratched their noses and sneezed over 10 minutes. Differences in serum IgE level changes were also assessed between the AR and control groups.

2.2 Histopathological analysis

Nasal specimens were obtained from both control mice and AR model mice. These specimens underwent fixation in 4% paraformaldehyde for 48 h, followed by decalcification using ethylenediaminetetraacetic acid (EDTA) over a 2-week period. Paraffin-embedded tissue specimens were serially processed through paraffin sectioning, xylene-based deparaffinization, and standard H & E histochemical protocols. Eosinophil counts were then determined within high-power fields of view (400×). At the same time, the thickness of the nasal mucosal epithelium in the olfactory region was measured.

2.3 Target identification and validation for active components

In accordance with our previous studies related to XCHD, active ingredients were retrieved from the TCMSP database (https://old.tcmspe.com/tcmsp.php) using oral bioavailability (OB ≥ 30%) and drug-likeness (DL ≥ 0.18) as primary screening criteria. The corresponding target proteins for all identified active ingredients were then mapped to the UniProt database (https://www.uniprot.org/), with the species specified as 'homosapiens'.

2.4 Disease potential target screening

Valid disease targets for 'allergic rhinitis' were defined as those retrieved from the GeneCards database (https://www.genecards.org/) with a Relevance score >1, after excluding duplicates.

2.5 Network analysis of herbal medicine components and their molecular targets

Using Cytoscape 3.10.1 software, we mapped the herbal components, bioactive compounds, and their respective therapeutic targets within XCHD to generate a network analysis diagram. Subsequently, the targets associated with XCHD's bioactive compounds were cross-referenced with known therapeutic targets for allergic rhinitis. This comparison identified overlapping targets, which were then visualized in a Venn diagram.

2.6 Overlapping results of active ingredient targets and potential targets of diseases in Chinese medicine compounds

The resultant interaction data were then visualized and subjected to hub gene identification through topological analysis using Cytohubba in Cytoscape platform (v3.10.1). Within cytohubba, the MCC algorithm was applied to identify the top 10 hub targets from the correlation rankings of the overlapping targets. The MCC algorithm was used to identify the top 10 related targets among the overlapping targets.

2.7 Enrichment and KEGG pathway analysis

Employing an integrative genomics approach, cross-validated targets mediating XCHD's anti-allergic rhinitis effects underwent functional annotation profiling (GO term classification) and canonical pathway network mapping (KEGG database) through ClusterProfiler's computational ontology framework.

2.8 Preparation of Xiaochaihu decoction

XCHD comprises seven herbs: Bupleurum chinense DC., Scutellaria baicalensis Georgi, Panax ginseng C.A. Mey., Pinellia ternate (Thunb.) Breit., Glycyrrhiza uralensis Fisch., Zingiber officinale Rosc, Ziziphus jujube Mill. The Kunming Dao Di Medicinal Materials Co. purchased all the herbs mentioned above. The XCHD extract was prepared by boiling water extraction to release bioactive components, following the doses specified in Table S1. Herbal materials were soaked in pure water at a 1 : 8 ratio for 30 minutes, then subjected to decoction for 40 minutes. After filtration to remove residues, this decoction process was repeated twice. The combined supernatants were then filtered, concentrated, and standardized to a final concentration of 3 g mL^{-1} for subsequent experiments.

The dose of XCHD administration was selected based on the combination of herbs in which XCHD is administered at a daily dose of 60 g in clinical practice. The equivalent dose administered was converted based on the ratio of human and mouse body surface area. The conversion factor between adults and mice was 9.1, and 7.8 g kg^{-1} was selected as the clinically equivalent dose.

Chemical composition of XCHD was characterized using UPLC-MS. After vortexing samples, 1 mL of each sample was transferred to an EP tube, evaporated to dryness in a high-speed vacuum centrifuge, and mixed with pre-chilled methanol. The mixture was then sonicated in an ice bath, incubated at −20 °C for 1 hour, centrifuged at 16 000 g at 4 °C for 20 min, and the supernatant was collected. The supernatant was evaporated to dryness in a high-speed vacuum concentrator. For mass spectrometry analysis, the sample was redissolved in 400 μL of pre-chilled methanol–water (1 : 1, v/v) solution, centrifuged at 20 000 g at 4 °C for 15 min, and an appropriate amount of supernatant was injected for analysis.

2.9 Immunohistochemistry analysis

The paraffin sections of nasal tissues were completely deparaffinized in xylene and antigenically repaired using sodium citrate. Sections were incubated with anti-matrix metalloproteinase 9 (MMP9) (1 : 200), anti-zonula occludens 1 (ZO-1) (1 : 500), anti-olfactory marker protein (OMP) primary antibody (1 : 200) overnight at 4 °C, and then with goat anti-mouse or goat anti-rabbit secondary antibodies for 2 h. Tissue sections were rinsed three times with PBS and subsequently stained with 4,6-

diamidino-2-phenylindole (DAPI). Fluorescence images were then acquired through confocal microscopy.

Post-anesthesia cardiothoracic irrigation procedures were executed in a PBS-4%PFA gradient sequence. Cerebral tissue stabilization in 4% PFA immersion with subsequent desiccation *via* hyperosmotic sucrose gradients (10–30% w/v sucrose). Brain sections 30 μm thick containing olfactory bulbs (OB) were cut using a frozen sectioning machine. Following closure in 5% bovine serum albumin with 0.1% Triton X-100 for 1 hour, the OB sections underwent overnight incubation at 4 °C with the primary antibody IBA-1 (diluted 1 : 500). Subsequently, the sections were incubated with species-aligned secondary antibody. Microglia were then visualized using confocal microscopy upon completion of the staining procedure.

2.10 RNA isolation and PCR analysis

PCR analysis was performed to analyze expression of MMP9, TNFα, IL-1β, and IL-6 in nasal mucosa tissues, and relative-mRNA in olfactory bulb tissues (Table S2). For both tissue types, total RNA was extracted with Trizol reagent, followed by reverse transcription to cDNA using PrimeScript RT Master Mix. qPCR was then carried out using Universal SYBR Green Fast qPCR Mix. GAPDH was used as the internal reference gene, and the relative expression of the target gene was determined by the $2^{-\triangle\triangle C_t}$ method.

2.11 Behavioral test

2.11.1 Buried food pellet test. The buried food pellet test (BFPT), which assesses olfactory thresholds, was employed to evaluate olfactory function in each group of mice. Twenty-four hours prior to testing, mice were fasted with water available ad libitum and habituated to the test cage for 10 minutes. The experiment involved randomly burying 200 g of regular food in the corners of a test cage containing 3 cm deep clean bedding. In each experiment, the latency to locate a food pellet was measured as the interval from when the mouse was placed randomly into the test cage until it found a pellet and grasped it with its front paws or teeth. This latency was recorded, and the test was terminated if the mouse failed to find a pellet within 300 seconds. Data were recorded at 300 s intervals. To serve as a control, a test with visible food pellets was implemented. Specifically, pelletized food was placed on the bedding surface, and the latency for the mice to discover the pellet was measured.

2.11.2 Open field test (OFT). Placing each experimental mouse gently in the center of a grey square plastic box (L40 cm × W40 cm × H30 cm), the mice's movement track was recorded and analyzed within 10 minutes using Ethovision software. The total distance moved by the mice, the speed of movement, time spent in the center zone, and number of center crossings were recorded. After each experiment, the apparatus was wiped with 70% alcohol.

2.11.3 Elevated plus maze (EPM). The elevated plus maze consists of two pairs of opposing arms, one pair open and one pair enclosed, intersecting at a central junction. Mice were placed at the maze center facing an open arm, with their 10-minute activity tracked by Ethovision. The analysis quantified the time spent in open arms (%) and entries into open arms relative to total arm visits.

2.11.4 Light–dark box. The light–dark box apparatus comprises two distinct compartments: one brightly illuminated and one dark. The illuminated compartment features white interior walls and is lit by overhead LED lights, contrasting with the dark compartment, which has black walls and no light source. An opening connects the two chambers, allowing mice to move freely between them. For testing, each mouse was initially positioned at the distal end of the illuminated compartment relative to the opening. Its behavior was then monitored and documented over a 10-minute period to evaluate both the frequency of transitions between compartments and the duration spent specifically within the illuminated area.

2.11.5 Tail suspension test (TST). The tail suspension test setup utilized a black acrylic enclosure featuring an overhead hook. Adhesive tape secured the distal portion of the mouse's tail, while the opposite end was affixed to the hook, thereby positioning the mouse in an inverted suspension within the chamber. Mouse activity was video-recorded over a 6-minute period, with immobility time quantified during the final 4 minutes.

2.11.6 Sucrose preference test (SPT). The mice were housed individually, provided with sufficient food, and habituated to a 2 percent sucrose solution. Provide the mice with two bottles containing either 2% sucrose solution or water. Weigh the bottles before and after the test. Water and sugar water consumption was determined by weighing the weight change of their bottles.

2.11.7 Forced swimming test (FST). The forced swimming test bucket is a transparent cylindrical bucket. Prior to testing, this container is filled with water maintained at approximately 25 °C and adjusted to a depth of roughly 18 cm. Mice are then gently introduced into the water. Researchers record the animals' activity duration over the entire 6-minute test period, specifically calculating the cumulative immobility time exhibited during the last 2 minutes.

2.12 Statistical analysis

Statistical analysis involved *t*-tests, one-way or two-way ANOVA followed by Tukey's post hoc tests, conducted in GraphPad Prism 9. Data are presented as mean ± standard error of the mean. The *P*-values <0.05*, <0.01**, and <0.001*** were accepted as a statistically significant.

3 Results

3.1 Establishment of OVA-induced AR mouse model

Model validation included examination of nasal mucosal eosinophil infiltration, assessment of nasal symptoms, and quantification of serum-specific IgE concentrations in mice with AR. HE staining revealed that the nasal mucosal epithelium of the control mice remained intact, exhibiting no significant pathological alterations. Relative to controls, the AR group exhibited prominent eosinophilic infiltration in the nasal

mucosa across all high-magnification fields (Fig. 1B and C). Quantitative analysis revealed that the olfactory epithelium (OE) thickness in the AR group was reduced compared to the control group, but no significant difference was observed (Fig. 1D). However, AR mice demonstrated marked elevations in both sneezing episodes and nasal grooming behaviors relative to baseline measures over the 10-min monitoring phase period (Fig. 1F and G). Immunological analysis further revealed markedly elevated serum levels of OVA-specific IgE in the AR group relative to controls (Fig. 1H). Collectively, these findings confirmed the successful generation of the AR model.

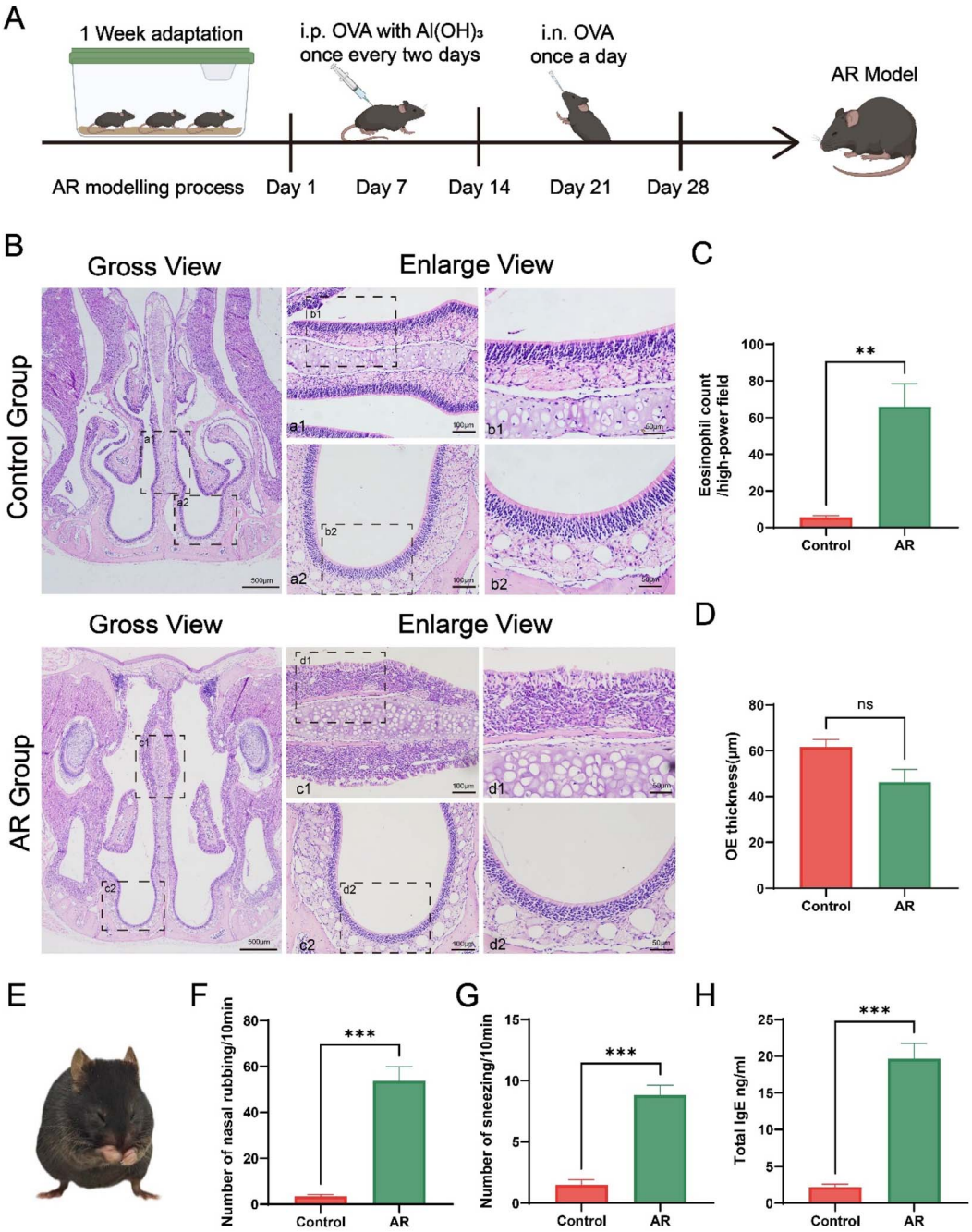

Fig. 1 Flowchart of establishing mouse model and confirmation of the successful establishment of AR model. (A) Experimental mice were first acclimatized for one week, and basic sensitization was achieved by intraperitoneal injection of OVA every two days in the AR group during days 1–14 after the start of the experiment. On days 15–28 of the experiment, 20 μL of OVA was injected by trans nasal drip at 2 pm daily for local excitation. (B) Representative HE staining images of the nasal mucosa of mice in each group (gross view, scale bar = 500 μm; enlarge view, scale bar = 100 μm, 50 μm). (C and D) Quantitative analysis of eosinophils in the nasal mucosa and thickness measurement analysis of the olfactory epithelium. (E) Schematic diagram of model mice. (F and G) Quantitative analysis of the number of nose scratching and sneezing in 10 min in control and AR groups. (H) Comparison of serum OVA-specific IgE levels between control and AR groups. *$p < 0.05$, **$p < 0.01$, ***$p < 0.001$.

3.2 Effective components of XCHD and screening of targets and pathways for the treatment of allergic rhinitis

XCHD, a widely utilized traditional Chinese medicine in clinics, is applied for analgesic, antipyretic, and anti-inflammatory treatments. The active ingredients in each herb in XCHD are 36 species of Scutellaria baicalensis Georgi, 13 species of Pinellia ternate (Thunb.) Breit., 17 species of Bupleurum chinense DC., 29 species of Ziziphus jujube Mill., 92 species of Glycyrrhiza uralensis Fisch., 22 species of Panax ginseng C.A. Mey., and 5 species of Zingiber officinale Rosc., respectively. After removing duplicate targets, we finally obtained 249 effective targets of XCHD. Utilizing Cytoscape software (version 3.10.1), we generated a network diagram (Fig. 2A) illustrating the relationships among herbal medicines, their active ingredients, and the corresponding protein targets.

To systematically characterize the chemical composition of XCHD, this research employed UPLC-MS technology for analysis in both positive and negative ion modes, identifying a total of 19 compounds (Table S4). Total ion chromatogram information is presented in Fig. S2A (positive ion mode) and Fig. S2B (negative ion mode). Flavonoids constitute a significant proportion of the overall composition. Based on their chemical characteristics, these compounds originate from the herbal ingredients in the Xiaochaihu Decoction formula, including Bupleurum chinense DC., Scutellaria baicalensis Georgi, Panax ginseng C.A. Mey., Pinellia ternate (Thunb.) Breit., Glycyrrhiza uralensis Fisch., Zingiber officinale Rosc, Ziziphus jujube Mill.

Targets associated with 'allergic rhinitis' (totaling 2221) were retrieved from the GeneCards database. Overlap analysis between XCHD active ingredient targets and allergic rhinitis-related targets yielded 100 shared targets (Fig. 2B). These shared targets are hypothesized to be central to the therapeutic action of XCHD against AR. Subsequently, we obtained the overlapping target interaction data using the string website and ranked them according to the degree of protein interaction (Fig. 2C and D).

To further explore the biological traits and associated pathways of the common genes, we utilized the 'ClusterProfiler' R package for GO and KEGG pathway enrichment analysis of the overlapping targets. The GO enrichment analysis categorized results into biological process (BP), molecular function (MF), and cellular component (CC). From the 2303 identified GO terms, the top 10 statistically significant ones were selected for visualization in a correlation bubble diagram (Fig. 2E). The analysis indicated that the overlapping targets between XCHD and AR were primarily involved in cellular responses to biotic stimuli, responses to molecules of bacterial origin (including lipopolysaccharide), responses to xenobiotic stimuli, and responses to decreased oxygen levels. For molecular functions, primary enrichment occurs in cytokine receptor binding, cytokine activity, growth factor receptor binding, ubiquitin-like protein ligase binding, and integrin binding. Regarding cellular components, significant enrichment is observed in plasma membrane raft, membrane raft, membrane microdomain, caveola, and vesicle lumen.

KEGG pathway analyses identified enrichment of relevant overlapping targets in 164 total pathways. Kyoto Encyclopedia of Genes and Genomes (KEGG) pathway enrichment analysis identified ten prioritized pathways (GeneRatio > 0.25), shown in the bubble plot (Fig. 2F) where bubble size indicates gene counts per pathway.

3.3 Core target identification and molecular docking

After importing the overlapping target interaction data into Cytoscape software, we obtained the top 10 core targets (Fig. 3A), which were IL1β, MMP9, IL6, TNF, STAT3, CASP3, AKT1, BCL2, IFNG, and ICAM1, respectively.

Based on the preceding results, molecular docking was performed on the targets MMP9, IL-1β, IL-6, and TNF using the top three effective compounds ranked by node degree—quercetin, kaempferol, and naringenin—as ligands. The chemical structures of the effective compounds are shown in Fig. S1. The requisite protein structures for these targets were sourced from the Protein Data Bank (PDB; https://www.rcsb.org/), while the ligand structures were obtained from the PubChem (*via* CID, (https://pubchem.ncbi.nlm.nih.gov/) and uniport databases. Optimal structures of small molecule ligands were searched using Chem3D software, and protein receptors were optimized using PyMol software. The best conformation was identified by importing the final structure into both AutoDockVina and PyMoL software.

Using AutoDockVina and PyMoL software, we molecularly docked Quercetin, Kaempferol, and Naringenin with MMP9, IL-1β, IL-6, and TNF (Fig. 3B–E). The effective binding energies of all analyzed dockings were less than -5 kcal mol^{-1}, suggesting that they are all well bound to each other (Table S3). The key compounds used in molecular docking were individually verified. UPLC-MS results confirmed that all three docking core components—Quercetin, Kaempferol, and Naringenin—were clearly detected in the actual XCHD samples (Table S4), primarily originating from the prescription herbs Scutellaria baicalensis Georgi or Glycyrrhiza uralensis Fisch.

3.4 XCHD repairs the nasal mucosal epithelial barrier and promotes olfactory recovery

The nasal mucosal epithelial barrier is essential in maintaining mucosal immune homeostasis, and to assess the potential effects of XCHD in treating AR, we examined barrier-related markers. Immunofluorescence analysis of ZO-1 revealed markedly reduced expression in the olfactory epithelium (OE) of AR mice compared to controls (Fig. 4B and C). This finding indicates that AR modeling impaired nasal mucosal tight junction (TJ) integrity. Furthermore, XCHD treatment upregulated TJ protein expression, partially restoring epithelial barrier function.

Previous results indicated that MMP9 is a primary therapeutic target of XCHD for AR treatment, participating in multiple physiological functions including tissue repair and immune response regulation. MMP9-mediated proteolytic cascade compromises blood–brain barrier (BBB) integrity through enzymatic degradation of structural components: (i)

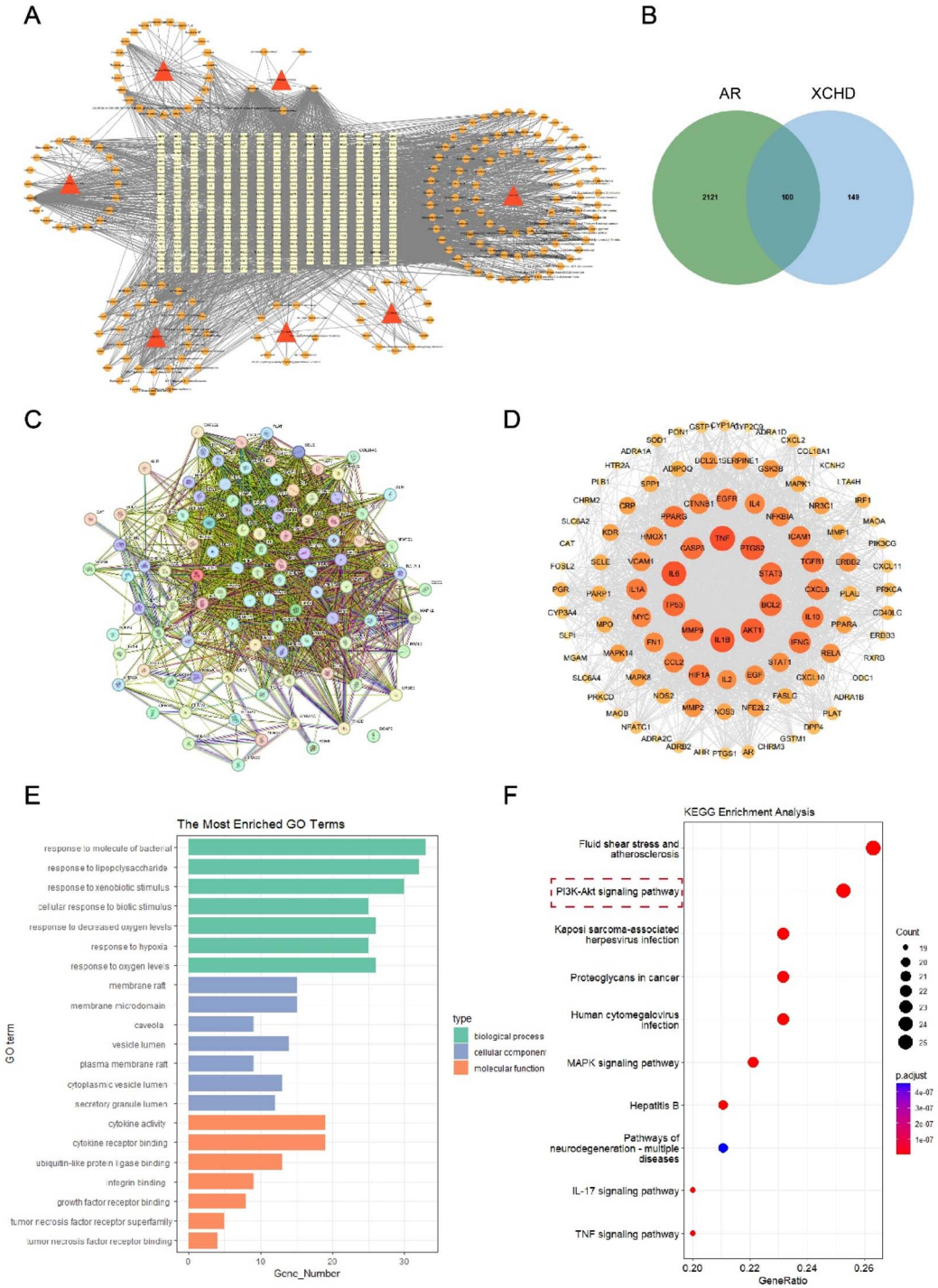

Fig. 2 Network pharmacological analysis of XCHD and AR-related targets. (A) Prescription-Herbal-ingredient-target network diagram. *V* is Prescription, the triangle is Herbal, the octagon is an ingredient, and the diamond is the target. The formula-TCM composition-target network diagram describes the relationship between TCM drug components and their targets. (B) Venn diagram of Xiaochaihu Decoction and allergic rhinitis. (C and D) Common targets between protein–protein interaction networks. Connections between nodes indicate protein–protein connections in the network. The size and color of the nodes are based on degree. From large to small, degree values follow a continuous mapping from red to yellow. (E) GO enrichment analysis of XCHD treatment of AR, including biological processes, molecular functions, and cellular components. (F) KEGG pathway analysis associated with the anti-allergic rhinitis effect of XCHD.

endothelial tight junction complexes (TJPs) and (ii) extracellular matrix proteins constituting the basal lamina. Subsequent paracellular permeability elevation permits transendothelial migration of peripheral monocytes/macrophages into the neural parenchyma. We therefore assessed MMP9 levels within the nasal mucosal barrier. Immunofluorescence analysis

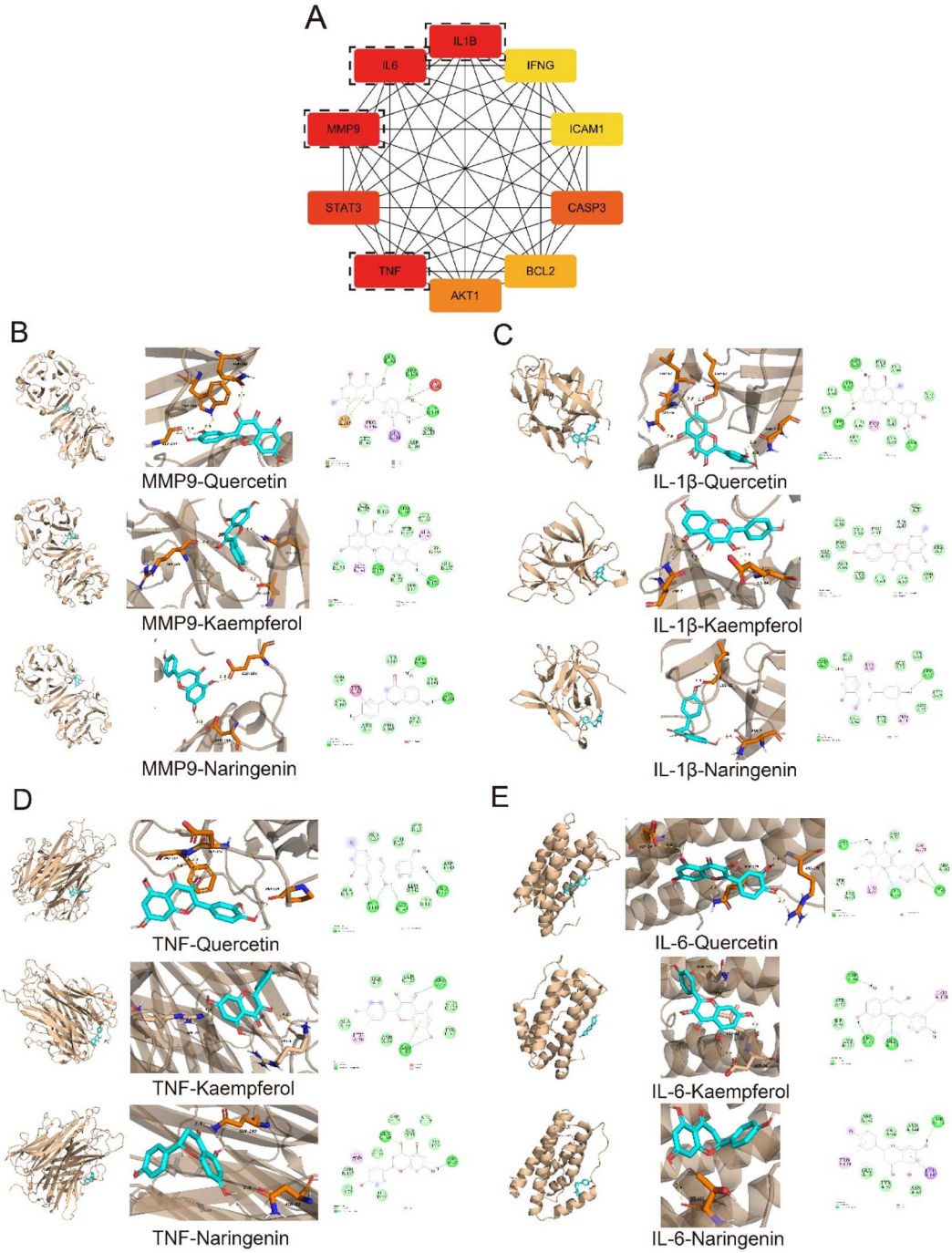

Fig. 3 Molecular docking of core targets with core components. (A) The top 10 core targets of XCHD were correlated with allergic rhinitis. (B–E) Molecular docking of Quercetin, Kaempferol, and Naringenin with target genes.

revealed a significant elevation in MMP9 protein within the olfactory epithelium (OE) of AR group mice compared to the control group (Fig. 4D and E). Furthermore, TNFα, IL6, and IL1β served as key inflammatory cytokines (Fig. 4F–I). Relative to the AR group, XCHD administration markedly lowered the mRNA expression of MMP9, IL6, IL1β, and TNFα. When blocking the PI3K pathway, the functional effects of XCHD are diminished.

OMP serves as a specific marker for olfactory receptor neurons and plays a crucial role in olfactory processing. We further performed immunofluorescence staining for OMP in the OE to assess mature OSN (Fig. 4J and K). In the control group, OMP showed intense red fluorescence in the OE because its expression in the olfactory epithelium was regular. In contrast to the control group, nasal allergic inflammation markedly suppressed OMP expression in the AR group. However, XCHD treatment enhanced OMP expression in the XCHD group.

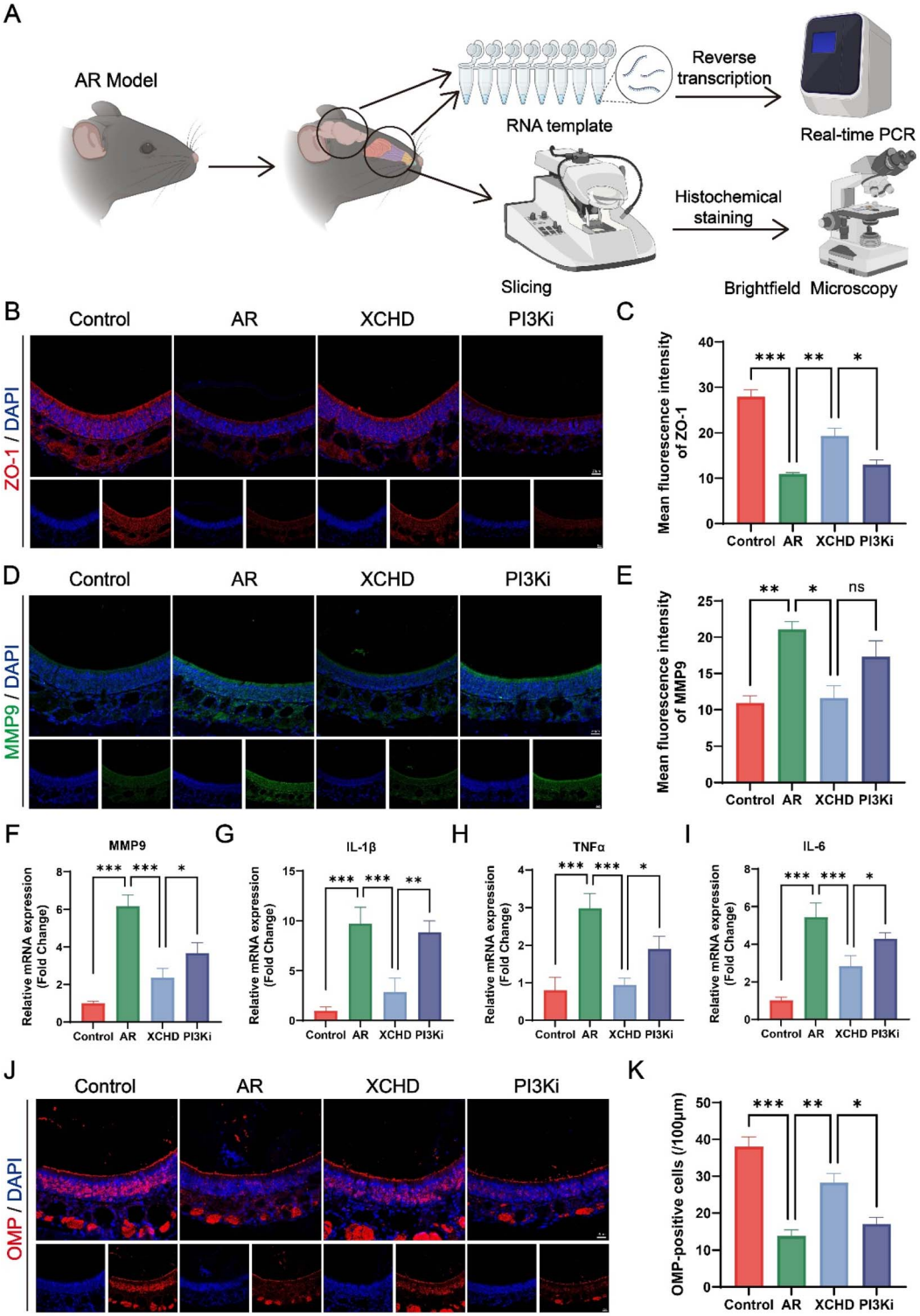

Fig. 4 Histopathological analysis of the effect of XCHD on the repair of nasal mucosal epithelium in allergic rhinitis mice and validation of the role of PI3K pathway. (A) Schematic illustration of the procedure of animal experiments. (B) Immunofluorescence staining to detect ZO-1 expression in nasal tissues. Blue, DAPI; red, ZO-1. (C) Quantitative analysis of ZO-1 immunofluorescence intensity. (D) Immunofluorescence staining to detect MMP9 expression in nasal tissues. Blue, DAPI; green, MMP9. (E) Quantitative analysis of MMP9 immunofluorescence intensity. (F–I) The effect of XCHD on the expression of MMP9, IL-1β, TNFα, and IL-6 mRNA in the nasal mucosa of mice was detected by PCR ($n = 3$, per group). (J) Immunofluorescence staining to detect OMP expression in nasal tissues. Blue, DAPI; red, OMP. (K) Quantification of the number of mature OSNs (OMP-positive neurons) in the OE of mice in each group. *$P < 0.05$, **$P < 0.01$, ***$P < 0.001$.

3.5 XCHD regulates neuroinflammation in the OB of AR mice

The olfactory bulb (OB) plays a pivotal role in transmitting AR-associated immune inflammation from the nasal cavity to the brain. To assess microglial activation within the OB, anti-IBA-1 antibody immunohistochemistry was employed. Findings revealed a significant elevation in IBA-1 expression in the OB of the AR group relative to the control group. Moreover, IBA-1-positive cells consistently exhibited enlarged cell bodies and thickened cytoplasmic protrusions (Fig. 5A). The level of microglia infiltration was higher in the lateral portion than in the medial portion, which was more prominent in the EPL, GL, and ONL layers (Fig. 5B–D). Notably, the number of microglia in the OB decreased after XCHD treatment, and the effect was more pronounced in the lateral portion. Moreover, the use of PI3K inhibitors significantly reduced the therapeutic effect of XCHD.

Considering the elevated levels of activation and infiltration of microglia in OB, we investigated the inflammatory response in AR mice. Expression analysis of key inflammatory factors indicated elevated levels of the pro-inflammatory cytokines TNFα, IL6, IL1β, and iNOS in the AR group (Fig. 5E–H). Administration of XCHD, however, significantly attenuated the expression of these cytokines.

3.6 XCHD modulates olfactory function in AR mice while regulating anxiety and depressive-like behaviour

Given the observed dysfunction in the olfactory epithelium and neuroinflammation in the OB of AR mice, we conducted olfactory behavioral tests to further evaluate their olfactory function. In the buried food test, we found that AR mice took more time to locate buried food particles than control mice, suggesting that AR mice may have impaired odor detection (Fig. 6C). Meanwhile, mice in the AR group exhibited a significantly shorter latency in locating food particles following XCHD treatment, indicating enhanced olfactory function. To verify the effect pathway of XCHD, a PI3K pathway inhibitor was

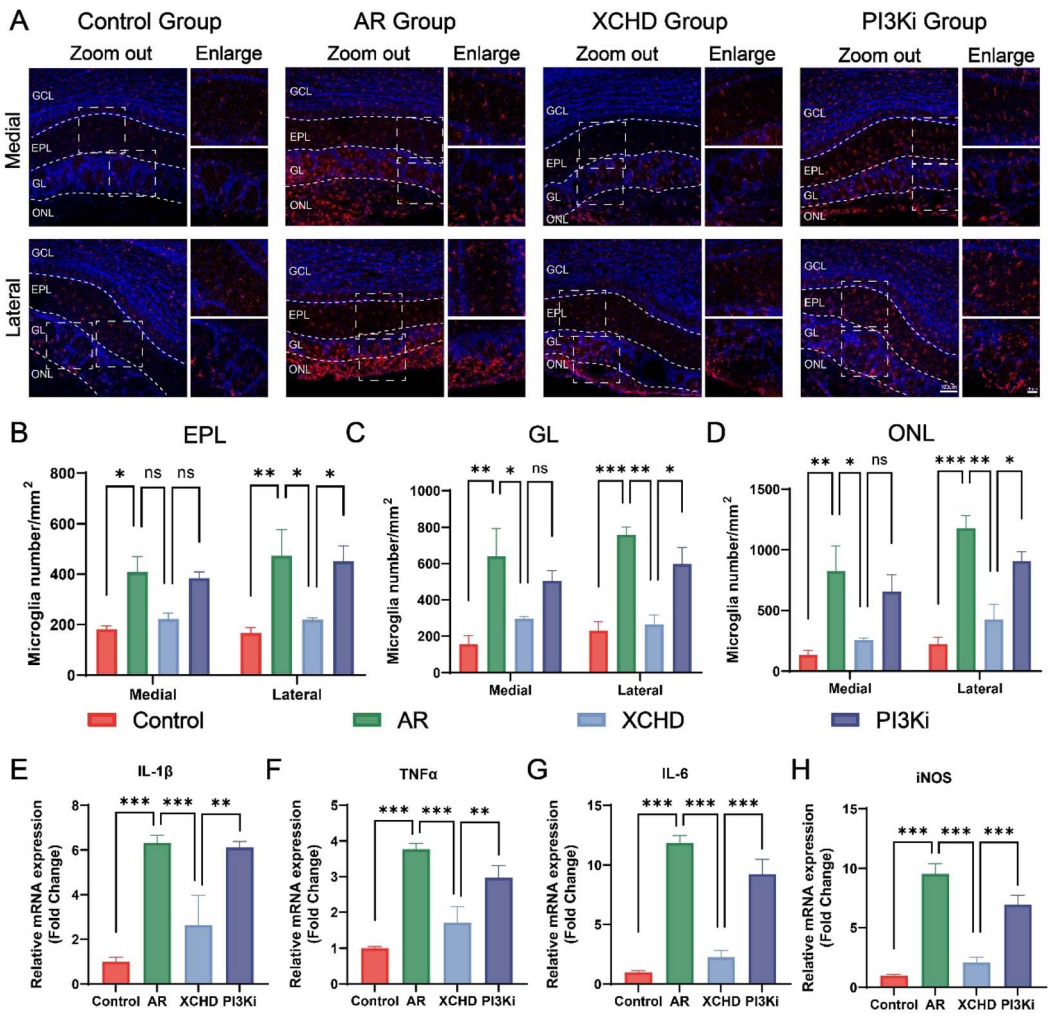

Fig. 5 Microglia activation and inflammation level detection in each group's OB mice. (A) Immunofluorescence staining (red) with anti-IBA-1 antibody shows activation and accumulation of microglia in ONL, GL, and EPL in each group's lateral and medial sides of OB. (B–D) Densitometric analysis of IBA-1 in EPL (B), GL (C), and ONL (D) of treated OBs in each group. (E–H) The effects of XCHD on IL-1β, TNFα, IL-6, and iNOS mRNA expression in mouse OBs were detected by PCR ($n = 3$, per group). *$P < 0.05$, **$P < 0.01$, ***$P < 0.001$.

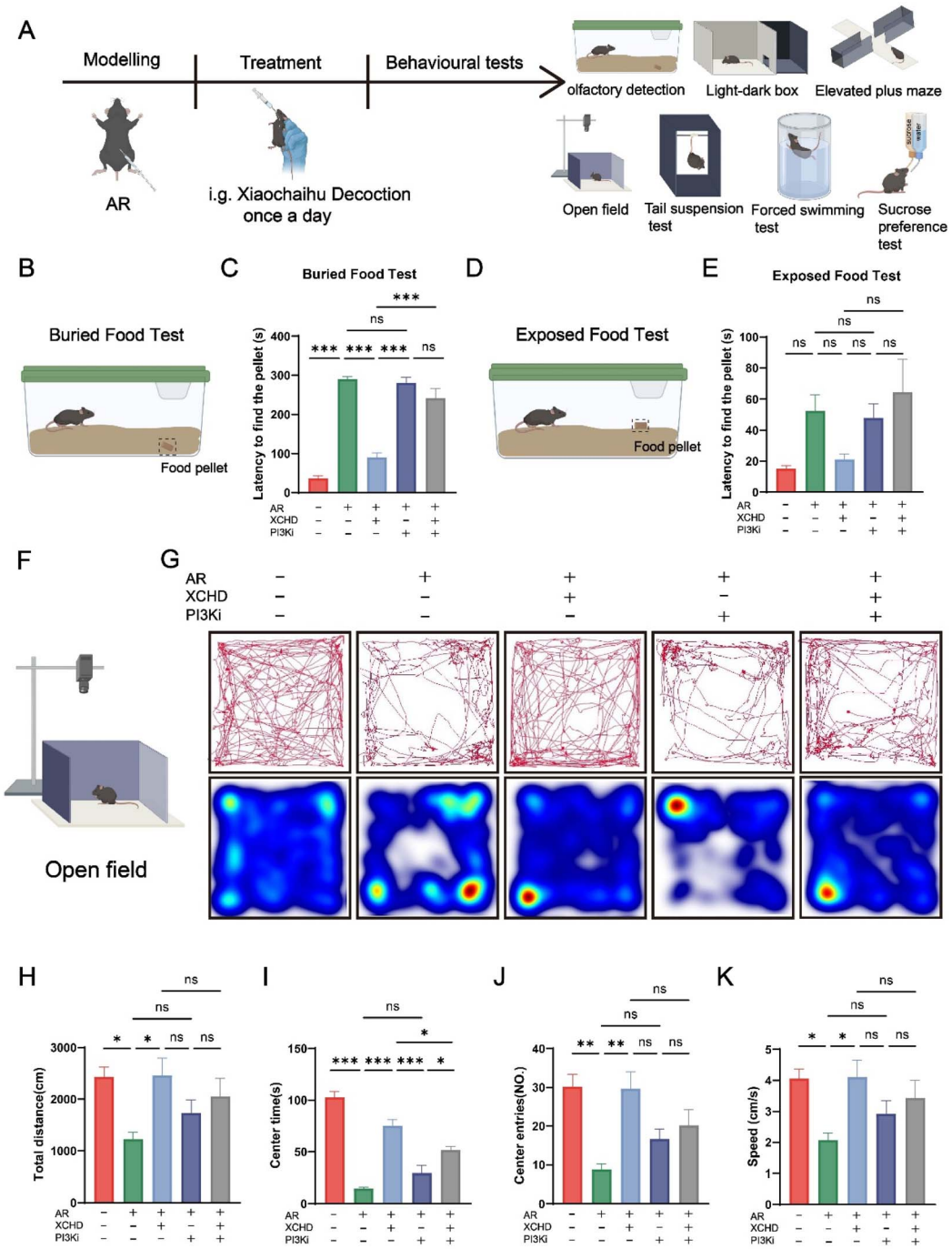

Fig. 6 Effects of XCHD on olfactory behavior and open field behavioral experiments in AR mice. (A) Schematic illustration of the procedure of behavioral experiments. (B) Schematic diagram illustrating the buried food pellet tests. (C) Quantification of latency to find a food pellet buried, ($n = 6$, per group). (D) Schematic diagram illustrating the visual food tests. (E) Quantification of latency to find a food pellet on the surface, ($n = 6$, per group). (F and G) Representative tracks in the open field experiment. (H–K) Quantitative analyses of total mouse distance moved (H), mouse movement speed (I), mouse central duration (J), and number of mouse central entries (K) in the open field experiment, respectively ($n = 6$, per group). *$P < 0.05$, **$P < 0.01$, ***$P < 0.001$.

employed. Results revealed that AR mice treated with XCHD exhibited further deterioration in olfactory function when subsequently treated with the inhibitor. In contrast, AR mice treated solely with the inhibitor showed no significant difference in olfactory function compared to the disease control group. As a control experiment, we conducted an exposed food experiment and found no difference in the latency to obtain food particles between the two groups of mice, indicating that the mice were not affected by motivation (Fig. 6E).

AR and its associated olfactory impairment are frequently linked to mental disorders. To assess anxiety-like and depressive behaviors in AR mice, we performed behavioral testing. Anxiety and depressive-like behaviors in mice were evaluated using the open field test. Relative to controls, AR mice showed significant decreases in total distance moved, average speed, time spent in the center, and frequency of center entries. This behavioral profile is consistent with severe anxiety and depression-like behaviors in the AR group (Fig. 6G–K). Compared with the AR group, mice treated with XCHD exhibited a significant increase in the number of entries into the center zone and the duration spent in this area. Additionally, their total distance traveled and average locomotor speed returned to levels comparable to controls, suggesting that XCHD administration mitigated anxiety- and depression-like behaviors in the mice. Meanwhile, further administration of PI3K inhibitors to XCHD-treated mice resulted in reduced residence time in the central area. AR mice treated with PI3K inhibitors alone still exhibited significant anxiety levels.

To further verify whether the mice had anxiety-like behaviors, we performed bright and dark boxes and elevated cross-maze tests. As illustrated in Fig. 7, AR mice exhibited a significant reduction in both bright box residence time and the total number of shuttles within the bright box relative to the control group. Following administration of XCHD, the residence time in the bright box increased in AR mice; however, the shuttle count remained comparable to that of the disease group (Fig. 7B and C). The XCHD-treated mice exhibited reduced time spent in the bright box following PI3K inhibitor administration, indicating that PI3K inhibitors partially suppress the therapeutic effects of XCHD.

In comparison to control cohorts, experimental subjects in the AR cohort displayed markedly reduced exploration of open maze quadrants, as decrease in open arm occupancy duration and fewer open compartment entries during elevated plus maze assessment, consistent with prototypical anxiety-related behavioral phenotypes (Fig. 7E). In contrast, the mean speed during movement tests in the maze did not differ significantly between groups, indicating that changes in motor function did not underlie the main effect (Fig. 7H). Behavioral analysis revealed that XCHD-treated mice displayed significantly prolonged open arm occupancy duration and exhibited an increased frequency of open arm entries relative to AR counterparts. PI3K inhibitors aggravated anxiety behavior in XCHD mice, but the effect was not very significant (Fig. 7F and G).

Anxiety and depression are modulated in overlapping pathways and co-occur in many patients. Therefore, we proceeded to explore the therapeutic effects of XCHD on depressive behavior. As indicated by the tail suspension test results, mice in the AR group exhibited a marked elevation in immobility duration relative to controls (Fig. 7J), implying greater susceptibility to depression induction. Conversely, XCHD administration significantly decreased immobility time compared to the AR group, demonstrating an amelioration of depressive symptoms. Data from the XCHD + PI3Ki group also differed significantly from the XCHD group, indicating a role for the PI3K pathway in mediating XCHD's therapeutic effects against depression.

A marked reduction in hedonic responsiveness was quantified through sucrose preference metrics, with AR-modeled mice demonstrating decrease in saccharide consumption ratio compared to untreated controls (Fig. 7L). Furthermore, the XCHD group exhibited a significantly elevated sucrose preference rate relative to the AR group, indicating XCHD's role in mitigating depression-like behaviors in AR mice. Of note, forced swimming test revealed no statistically significant difference between the AR and control groups (Fig. S3).

These findings indicate that XCHD partially mitigates the marked depressive-like behaviors observed in AR group mice. At the same time, the PI3K inhibitor can inhibit some of the therapeutic effects of XCHD. When AR mice were treated solely with PI3K inhibitors, no significant changes in anxiety or depression levels were observed.

4 Discussion

Allergic rhinitis is a prevalent and multifaceted chronic inflammatory condition driven by IgE, triggered upon exposure to specific allergens in susceptible individuals. Presently, pharmacotherapy constitutes the cornerstone of AR management, where a polypharmacy approach is critical for managing symptoms and preventing recurrence.[17] Therefore, it is important to explore better medication strategies and develop new pharmacological interventions to improve the management of AR. Recent years have seen growing recognition of Traditional Chinese Medicine's (TCM) role in treating AR, with research into its therapeutic mechanisms becoming a significant focus.[18]

As a traditional compound herbal medicine, XCHD demonstrates multi-target engagement and elicits diverse cytoprotective responses, encompassing antioxidative and anti-inflammatory actions. In addition, researchers have shown that XCHD can treat neurological-related disorders, such as depression. However, the therapeutic effect of XCHD in AR remains unexplored. Consequently, network pharmacological strategies combined with computational docking approaches were implemented to characterize XCHD's anti-allergic mechanisms. Our findings indicate that MMP9, IL-1β, IL-6, and TNF represent the key therapeutic targets of XCHD for AR treatment. Meanwhile, the PI3K pathway may play a crucial role in the therapeutic efficacy of XCHD.

The key target of XCHD for AR was experimentally validated in this research. Restoration of the nasal mucosal epithelial barrier, important in maintaining mucosal immune homeostasis, is considered a therapeutic approach for AR. MMP9 participates in critical physiological functions, including tissue repair, angiogenesis, and immune response modulation.[19] However, its dysregulation is primarily associated with inflammatory diseases. Significantly, MMP9 compromises blood–brain barrier (BBB) integrity by degrading components of the basement membrane critical for tight junction proteins (TJPs) and BBB structure.[20,21] In addition, disruption of the tight junctions of the nasal mucosa lowers the threshold for allergen exposure. It can susceptibly lead to allergen sensitization, leading to local antigen-driven inflammation. Among them, ZO-1 is the major scaffolding protein of the tight junctions.[22] Our

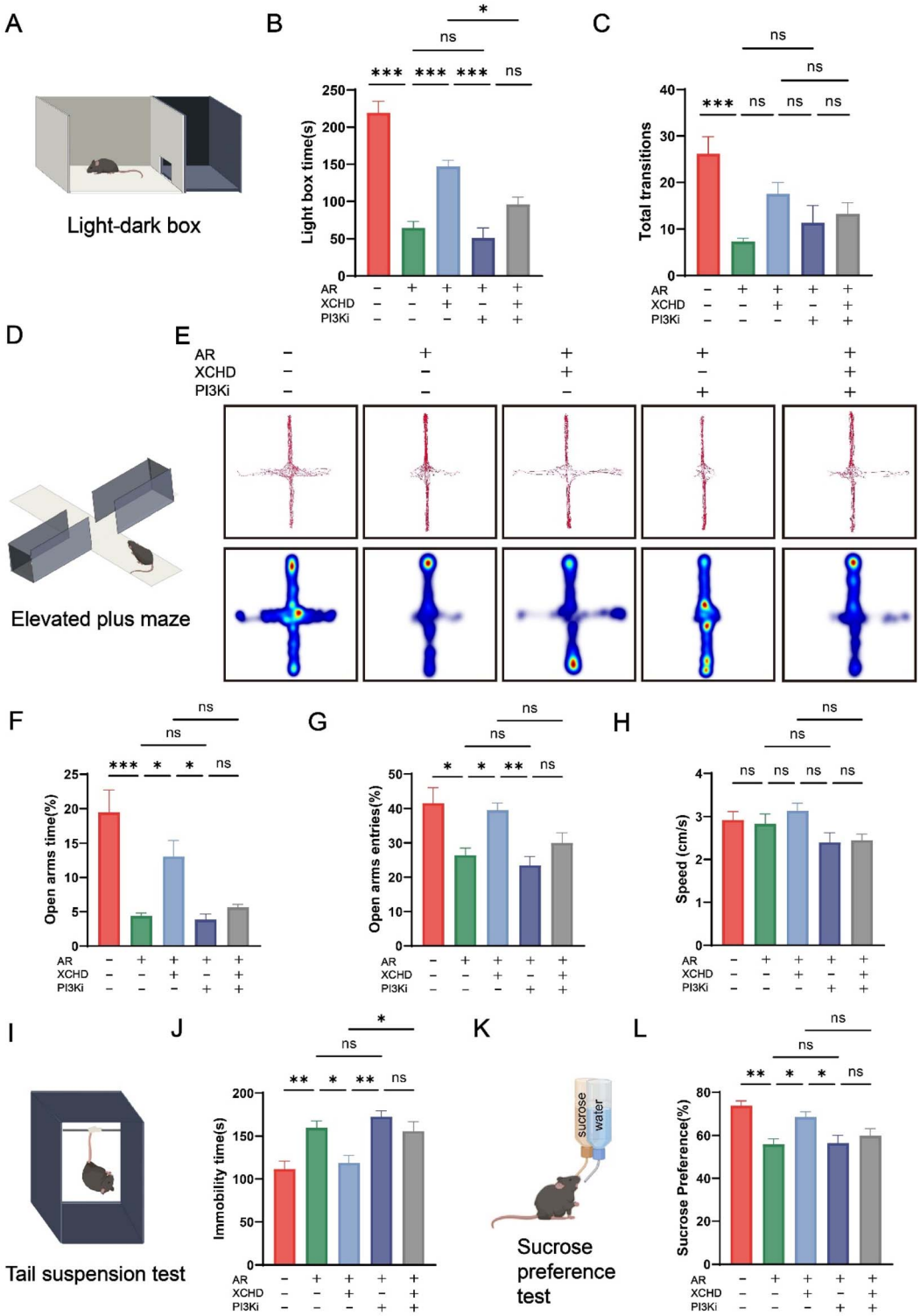

Fig. 7 Effects of XCHD on anxiety and depression-like behavior in AR mice (A) Schematic diagram illustrating the Light–dark box test. (B–C) Quantitative analyses of duration (B) and number of shuttles (C) in the light–dark box from mice, respectively ($n = 6$, per group). (D and E) Representative tracks in elevated cross maze test from mice. (F–H) Quantitative analyses of the percentage of duration (F), percentage of number of entries into open arms (G), and speed of movement (H) in the elevated cross maze, respectively, ($n = 6$, per group). (I) Schematic diagram illustrating the tail suspension test. (J) Quantitative analyses of the immobility time in the tail suspension test, ($n = 6$, per group). (K) Schematic diagram illustrating the sucrose preference test. (L) Quantitative analyses of the rate of sucrose preference, ($n = 6$, per group). *$P < 0.05$, **$P < 0.01$, ***$P < 0.001$.

findings demonstrate diminished expression levels of MMP9 and ZO-1 in the AR group, indicating compromised nasal mucosal barrier function. Significantly, XCHD administration effectively lowered MMP9 levels while concurrently elevating the expression of tight junction proteins, thereby enhancing the integrity of cell–cell junctions within the nasal epithelial barrier.

Based on the above findings, a compromised nasal mucosal barrier could facilitate the entry of inflammatory cells and other detrimental agents into the olfactory bulb *via* the brain-nose axis, inducing glial cell activation and a neuroinflammatory response.[23] Using PCR, we assessed the expression levels of inflammatory factors (IL-1β, IL-6, TNFα) in the nasal mucosa and olfactory bulb. XCHD's pharmacological effect was evidenced by decreased cytokine levels in AR models. This finding further validates XCHD as a potential therapeutic target in AR.

AR has long been one of the major causes of clinical olfactory disorders. However, the mechanism of AR-associated OD is still unclear, and it is usually thought to be related to the inflammatory component or impairment of the conduction process. Clinical practice has revealed that anti-inflammatory treatment can attenuate OD in patients with AR. Meanwhile, the OB, serving as the initial processing center in the olfactory pathway, contributes to the pathogenesis of OD associated with allergic rhinitis.[24]

Damage and inflammation of olfactory epithelial cells, triggered by inflammatory factor infiltration in the nasal olfactory region's mucosal epithelium, can impair the function and reduce the number of olfactory receptor neurons.[25] To validate this effect, the research showed that OMP expression was significantly reduced in the AR group compared to the control group. Conversely, OMP expression was restored following XCHD treatment. Next, we sought to compare the behavioral results of the olfactory function tests in each group to assess the extent of OD. We found that the AR group had a significantly longer time to detect food particles than the control group, while the XCHD group had a significantly improved OD. The above results suggest that using XCHD effectively alleviates OD in AR patients, which is consistent with the histological staining results. In addition, the recovery of OMP expression was closely related to functional recovery. In addition to inflammation of the nasal mucosa, OB neuroinflammation caused by chronic rhinitis has been widely investigated. Because OB inflammation is not only an important cause of OD but may also cause AR-related anxiety and other mood disorders.[26,27] In the AR group, microglia in both the lateral and medial portions of the OB showed an activated state, with a more significant accumulation of ONL, GL, and EPL. Following XCHD treatment, a significant reduction in olfactory bulb microglia count was observed, alongside a decreased proportion of activated microglia. Consistent with previous findings, XCHD partially restores olfactory function in AR mice, likely by reducing inflammatory responses in the nasal mucosa and olfactory bulb.

Extensive research indicates that individuals with peripheral inflammatory disorders exhibit an increased propensity to develop depressive symptoms. This heightened vulnerability is attributed to heightened concentrations of inflammatory mediators.[28] Functioning as the primary gateway for substances entering the brain from the nasal cavity, the OB serves as a critical factor in the pathogenesis of mood disorders. The behavioral assessment in this research revealed that AR mice exhibited significant anxiety and depression-like behaviors. Notably, behavioral improvement was observed in XCHD-treated subjects, with marked increases in central zone occupancy time and exploratory entries during OFT. Furthermore, in the elevated plus maze, XCHD administration resulted in a significant increase in both the proportion of time spent in the open arms and the number of open arm entries. An increase in time spent in the bright chamber was also observed in the light–dark box test. Meanwhile, XCHD markedly reduced immobility duration in the TST and enhanced sucrose preference in AR mice. Collectively, these data demonstrate that XCHD can moderately ameliorate anxiety-depression-like behaviors in AR mice.

Based on histological and behavioral assessments, *in vivo* administration of PI3K inhibitors significantly attenuated the efficacy of XCHD in promoting olfactory function recovery and alleviating depression-like behaviors in the AR model. When PI3K inhibitors were administered alone to the AR model, no recovery or worsening of olfactory or emotional deficits was observed in AR mice. These findings suggest that the PI3K-Akt pathway may be involved in the therapeutic mechanism of XCHD.

Although this research reveals the potential role of XCHD in improving AR-related symptoms, some limitations remain. Based on an animal model, the findings provide meaningful insights into possible mechanisms. However, it remains to be seen whether these results can be applied to human patients, as further validation is required. Furthermore, our data only suggest that the PI3K pathway may play a significant role in XCHD's therapeutic efficacy, but other pathways may also be involved. This aspect requires further confirmation through additional biological experiments in subsequent studies.

5 Conclusion

This research suggests that XCHD may regulate AR through the synergistic interactions of its multiple components, which appear to converge on key targets within the PI3K-Akt signaling pathway. XCHD alleviates the olfactory dysfunction and emotional abnormality associated with AR through the dual mechanisms of mucosal repair and neural anti-inflammation, which alleviates the limitations of the lack of clinical interventions for AR mood disorders. Given the potential of traditional Chinese medicine formulations to reduce the risk of resistance development, XCHD may represent a promising therapeutic strategy for managing allergic rhinitis, with potential implications for future clinical application.

Author's contributions

Yiyi Lin: conceptualization, writing, methodology, investigation, summarizing data; Shihan Liu: visualization; Zhiquan Zhu: summarizing data; Jinxiong Yang: formal analysis; Pan

Huang: investigation softwar; Yuyang Liu: supervision; Wenlong Luo: project administration.

Conflicts of interest

The authors declare that they have no known competing financial interests or personal relationships that could have appeared to influence the work reported in this paper.

Abbreviations

AR	Allergic rhinitis
TCM	Traditional Chinese medicine
XCHD	Xiaochaihu decoction
OVA	Ovalbumin
OD	Olfactory dysfunction
EDTA	Ethylenediaminetetraacetic acid
HE	Hematoxylin-eosin
GO	Gene ontology
KEGG	Kyoto encyclopedia of genes and genomes
BP	Biological process
MF	Molecular function
CC	Cellular component
MMP9	Matrix metalloproteinase 9
ZO-1	Zonula occludens-1
OMP	Olfactory marker protein
DAPI	4,6-Diamidino-2-phenylindole
PFA	Paraformaldehyde
OB	Olfactory bulbs
BFPT	Buried food pellet test
OFT	Open field test
EPM	Elevated plus maze
ANOVA	Analysis of variance
PDB	Protein data bank
TJs	Tight junctions
TJPs	Tight junction proteins
BBB	Blood–brain barrier
TST	Tail suspension test
SPT	Sucrose preference test
FST	Forced swimming test

Data availability

Data will be made available on request.

Supplementary information (SI) is available. See DOI: https://doi.org/10.1039/d5ra09128d.

References

1 J. A. Bernstein, J. S. Bernstein, R. Makol, *et al.*, Allergic rhinitis: a review, *Jama*, 2024, **331**(10), 866–877.
2 Y. Zhang, F. Lan and L. Zhang, Advances and highlights in allergic rhinitis, *Allergy*, 2021, **76**(11), 3383–3389.
3 X. Zhang, Y. Zhou, Z. Liu, *et al.*, Olfactory Dysfunction in Allergic Rhinitis, *Clin. Rev. Allergy Immunol.*, 2024, **68**(1), 3.
4 F. M. Passali, G. C. Passali, D. Passali, *et al.*, Smell impairment in patients with allergic rhinitis[C], *Int. Forum Allergy Rhinol.*, 2021, **11**(6), 1031–1032.
5 K. B. Patel, J. W. Mims and J. D. Clinger, The burden of asthma and allergic rhinitis: epidemiology and health care costs, *Otolaryngol. Clin.*, 2024, **57**(2), 179–189.
6 P. Liu, D. Qin, H. Lv, *et al.*, Neuroprotective effects of dopamine D2 receptor agonist on neuroinflammatory injury in olfactory bulb neurons *in vitro* and *in vivo* in a mouse model of allergic rhinitis, *Neurotoxicology*, 2021, **87**, 174–181.
7 X. Zhang, Y. Zhou, Z. Liu, *et al.*, Olfactory Dysfunction in Allergic Rhinitis, *Clin. Rev. Allergy Immunol.*, 2024, **68**(1), 3.
8 J. Rodrigues, F. Franco-Pego, B. Sousa-Pinto, *et al.*, Anxiety and depression risk in patients with allergic rhinitis: a systematic review and meta-analysis, *Rhinology*, 2021, **59**(4), 360–373.
9 J. Rodrigues, J. V. Pinto, P. L. Alexandre, *et al.*, Allergic rhinitis seasonality, severity, and disease control influence anxiety and depression, *Laryngoscope*, 2023, **133**(6), 1321–1327.
10 M. Bedolla-Barajas, J. Morales-Romero, N. A. Pulido-Guillén, *et al.*, Rhinitis as an associated factor for anxiety and depression amongst adults, *Braz. J. Otorhinolaryngol.*, 2017, **83**, 432–438.
11 J. Ma, F. Wang, J. Yang, *et al.*, Xiaochaihutang attenuates depressive/anxiety-like behaviors of social isolation-reared mice by regulating monoaminergic system, neurogenesis and BDNF expression, *J. Ethnopharmacol.*, 2017, **208**, 94–104.
12 J. Dai, J. Yang and C. Li, Transport and metabolism of flavonoids from Chinese herbal remedy Xiaochaihu-tang across human intestinal Caco-2 cell monolayers, *Acta Pharmacol. Sin.*, 2008, **29**(9), 1086–1093.
13 J. Li, R. Hu, S. Xu, *et al.*, Xiaochaihutang attenuates liver fibrosis by activation of Nrf2 pathway in rats, *Biomed. Pharmacother.*, 2017, **96**, 847–853.
14 S. Shao, R. Jia, L. Zhao, *et al.*, Xiao-Chai-Hu-Tang ameliorates tumor growth in cancer comorbid depressive symptoms *via* modulating gut microbiota-mediated TLR4/MyD88/NF-κB signaling pathway, *Phytomedicine*, 2021, **88**, 153606.
15 J. Ma, C. F. Wu, F. Wang, *et al.*, Neurological mechanism of Xiaochaihutang's antidepressant-like effects to socially isolated adult rats, *J. Pharm. Pharmacol.*, 2016, **68**(10), 1340–1349.
16 X. Yu, W. Qin, H. Cai, *et al.*, Analyzing the molecular mechanism of xuefuzhuyu decoction in the treatment of pulmonary hypertension with network pharmacology and bioinformatics and verifying molecular docking, *Comput. Biol. Med.*, 2024, **169**, 107863.
17 L. Klimek, J. Mullol, A. K. Ellis, *et al.*, Current management of allergic rhinitis, *J. Allergy Clin. Immunol.:Pract.*, 2024, **12**(6), 1399–1412.
18 H. H. L. Chan and T. Ng, Traditional Chinese medicine (TCM) and allergic diseases, *Curr. Allergy Asthma Rep.*, 2020, **20**, 1–18.
19 H. Chi, Z. Dong, Q. Gan, *et al.*, Matrix metalloproteinase 9 modulates immune response along with the formation of

extracellular traps in flounder (Paralichthys olivaceus), *Fish Shellfish Immunol.*, 2023, **133**, 108570.

20 F. Takata, S. Nakagawa, J. Matsumoto, *et al.*, Blood–brain barrier dysfunction amplifies the development of neuroinflammation: understanding of cellular events in brain microvascular endothelial cells for prevention and treatment of BBB dysfunction, *Front. Cell. Neurosci.*, 2021, **15**, 661838.

21 H. Zailani, W. L. Wang, S. K. Satyanarayanan, *et al.*, Omega-3 polyunsaturated fatty acids and blood–brain barrier integrity in major depressive disorder: restoring balance for neuroinflammation and neuroprotection, *Yale J. Biol. Med.*, 2024, **97**(3), 349.

22 W. T. Kuo, L. Zuo, M. A. Odenwald, *et al.*, The tight junction protein ZO-1 is dispensable for barrier function but critical for effective mucosal repair, *Gastroenterology*, 2021, **161**(6), 1924–1939.

23 S. Hasegawa-Ishii, A. Shimada and F. Imamura, Lipopolysaccharide-initiated persistent rhinitis causes gliosis and synaptic loss in the olfactory bulb, *Sci. Rep.*, 2017, **7**(1), 11605.

24 C. Ren, Y. K. Mou, X. Y. Song, *et al.*, P2X7 receptor of microglia in olfactory bulb mediates the pathogenesis of olfactory dysfunction in a mouse model of allergic rhinitis, *Faseb. J.*, 2023, **37**(6), e22955.

25 J. H. Turner, L. May, R. R. Reed, *et al.*, Reversible loss of neuronal marker protein expression in a transgenic mouse model for sinusitis-associated olfactory dysfunction, *Am. J. Rhinol. allergy*, 2010, **24**(3), 192–196.

26 Y. Mou, C. Sun, S. Wei, *et al.*, P2X7 receptor of olfactory bulb microglia plays a pathogenic role in stress-related depression in mice with allergic rhinitis, *Neurobiol. Dis.*, 2024, **192**, 106432.

27 Z. Gao, H. Lv, Y. Wang, *et al.*, TET2 deficiency promotes anxiety and depression-like behaviors by activating NLRP3/IL-1β pathway in microglia of allergic rhinitis mice, *Mol. Med.*, 2023, **29**(1), 160.

28 B. Guo, M. Zhang, W. Hao, *et al.*, Neuroinflammation mechanisms of neuromodulation therapies for anxiety and depression, *Transl. Psychiatry*, 2023, **13**(1), 5.